

Can we define a unique microscopic pressure in inhomogeneous fluids?

Cite as: J. Chem. Phys. 154, 084502 (2021); <https://doi.org/10.1063/5.0044487>

Submitted: 16 January 2021 . Accepted: 25 January 2021 . Published Online: 22 February 2021

 Kaihang Shi,  Erik E. Santiso, and  Keith E. Gubbins



View Online



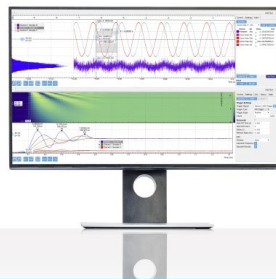
Export Citation



CrossMark

Challenge us.

What are your needs for
periodic signal detection?



Zurich
Instruments

Can we define a unique microscopic pressure in inhomogeneous fluids?

Cite as: J. Chem. Phys. 154, 084502 (2021); doi: 10.1063/5.0044487

Submitted: 16 January 2021 • Accepted: 25 January 2021 •

Published Online: 22 February 2021



View Online



Export Citation



CrossMark

Kaihang Shi,^{a),b)} Erik E. Santiso,^{b)} and Keith E. Gubbins^{b)}

AFFILIATIONS

Department of Chemical and Biomolecular Engineering, North Carolina State University, Raleigh, North Carolina 27606, USA

^{a)}**Current address:** Department of Chemical and Biological Engineering, Northwestern University, Evanston, IL 60208, USA.

^{b)}**Authors to whom correspondence should be addressed:** kaihangshi0@gmail.com; eesantis@ncsu.edu; and keg@ncsu.edu

ABSTRACT

The estimation of a microscopic pressure tensor in an adsorbed thin film on a planar surface remains a challenge in both experiment and theory. While the normal pressure is well-defined for a planar surface, the tangential pressure at a point is not uniquely defined at the nanoscale. We report a new method that allows us to calculate the local pressure tensor and its spatial integral using an arbitrary contour definition of the “virial-route” local pressure tensor. We show that by integrating the local tangential pressure over a small region of space, roughly the range of the intermolecular forces, it is possible to define a coarse-grained tangential pressure that appears to be unique and free from ambiguities in the definition of the local pressure tensor. We support our argument by presenting the results for more than ten types of contour definitions of the local pressure tensor. By defining the coarse-grained tangential pressure, we can also find the effective thickness of the adsorbed layer and, in the case of a porous material, the statistical pore width. The coarse-grained in-layer and in-pore tangential pressures are determined for Lennard-Jones argon adsorbed in realistic carbon slit pores, providing a better understanding of the pressure enhancement for strongly wetting systems.

Published under license by AIP Publishing. <https://doi.org/10.1063/5.0044487>

I. INTRODUCTION

For a small system that is in thermodynamic equilibrium with a bulk fluid phase, such as an adsorbate within a nano-porous adsorbent, a small liquid drop, or a nanoparticle, many thermodynamic functions are not uniquely defined at the nanoscale. Using the classification of thermodynamic variables introduced by Griffiths and Wheeler,¹ the “field” variables (variables that take the same values in two or more coexisting phases) are well-defined at all scales; for the examples cited, the field variables are the temperature and the chemical potentials. However, the “densities” (first derivatives of the thermodynamic potential, such as the specific volume, specific entropy, pressure, or number density) are usually not uniquely defined. Familiar cases include the volume or density of adsorbate molecules within a narrow pore. If we focus on the adsorbed nano-phase as the system, we must define a system boundary. For a narrow pore in a solid, two common choices are to draw the boundary through the nuclei of the atoms on the solid surface that forms the pore wall (the “physical width,” as determined by neutron

diffraction, for example) or to define a boundary that allows for “dead space” near the wall, which is impenetrable to adsorbate molecular centers under normal conditions (the “effective width”). For argon in narrow pores of the order, say, 1 nm width, these two definitions of pore volume are quite different; for a carbon pore of 1 nm physical width, the effective width is about 0.42 nm so that the physical width is more than twice the effective one. The pressure is similarly non-unique at very small scales. In the case of the pressure, the reason for the non-uniqueness arises because there is no unique way to assign the pair forces between molecules to a particular point in space.² This seems to have been apparent to both Maxwell³ and Boltzmann⁴ in the nineteenth century, although their discussion was mostly focused on violations of the second law.

Despite the non-uniqueness at the nanoscale, once the system boundary is chosen, the volume can often be determined experimentally, from diffraction or adsorption measurements, for example. The non-uniqueness of the local pressure for an adsorbed layer or nano-phase is more subtle. Because of the inhomogeneity, the

pressure, \mathbf{P} , is a second-order tensor, with component $P_{\alpha\beta}$ giving the force per unit area in the β -direction acting on a surface-element normal to the α -direction. In the absence of external fields, the condition of mechanical equilibrium is given by the gradient of the pressure tensor,⁵

$$\nabla \cdot \mathbf{P} = 0. \quad (1)$$

Although the gradient of \mathbf{P} is well-defined, this is insufficient to uniquely define \mathbf{P} itself. The local pressure tensor is the sum of a kinetic (ideal gas) part and a configurational (due to intermolecular forces) part, $\mathbf{P}(\mathbf{r}) = \mathbf{P}^K(\mathbf{r}) + \mathbf{P}^C(\mathbf{r})$, where the kinetic pressure tensor is well-defined and is given by $\mathbf{P}^K(\mathbf{r}) = \rho(\mathbf{r})k_B T \mathbf{1}$, where $\rho(\mathbf{r})$ is the molecular number density at a point \mathbf{r} , k_B is the Boltzmann constant, T is the temperature, and $\mathbf{1}$ is the second-order unit tensor. However, the configurational contribution, $\mathbf{P}^C(\mathbf{r})$, by the virial (or mechanical) route^{2,3} involves an integration over an arbitrarily defined contour path connecting the center of mass of two molecules at locations \mathbf{r}_i and \mathbf{r}_j (see Sec. II A). This difficulty was first recognized by Irving and Kirkwood (IK) in their paper in 1950.² “This definition of the force ‘acting across dS ’ is quite arbitrary, and with another definition we would obtain a different expression for the point function stress tensor. But all definitions must have this in common—that the stress between a pair of molecules be concentrated near the line of centers.” The local stress tensor at time t , $\sigma(\mathbf{r}, t)$, is related to the local pressure tensor by $\langle \sigma(\mathbf{r}, t) \rangle = -\mathbf{P}(\mathbf{r})$, where $\langle \dots \rangle$ denotes the ensemble average; IK defined the contour to be a straight line connecting centers of molecules (i.e., Irving–Kirkwood or IK definition). Alternative, but equally valid, contour definitions are possible; a popular choice is that of Harasima,^{6,7} the definition of which is composed of two orthogonal line segments in planar geometry. Many efforts have been devoted over the past few decades in the hope of finding a unique expression for the local pressure/stress tensor. Mistura⁸ argued that the local pressure tensor can be uniquely defined by the IK definition but made an unjustified assumption that the contour path is physically equivalent to the shortest distance (straight line) between two molecules. Later, Baus and Lovett⁹ claimed that the ambiguity in the local stress tensor can be eliminated by imposing St. Venant’s condition. However, Rowlinson¹⁰ immediately pointed out that the Baus–Lovett formulation leads to a vanishing surface tension, and Rowlinson’s argument, in our opinion, has not been convincingly refuted by Baus and Lovett in their follow-up publications.^{11,12} Wajnryb *et al.*¹³ concluded that the IK definition is the unique choice by imposing additional conditions (e.g., symmetry and translational and rotational invariance) on the tensor. However, the authors implicitly considered the IK definition as the only valid choice of contour during their proof; similar concerns about the work were also raised by Hafskjold and Ikeshoji.¹⁴ Recently, Rossi and Testa¹⁵ argued that if the stress tensor is identified as the tensor that multiplies the deformation tensor to express the work done by the system under an infinitesimal local deformation, such a local stress tensor is then uniquely defined, and it has an appearance similar to the Harasima definition. Until now, no consensus has been reached in the field on the uniqueness of the local pressure tensor, and there is no convincing general justification for choosing one contour definition over the other. The thermodynamic route^{16–19} to the local pressure tensor suffers the same issue as the virial one because there are an infinite number of

ways to distribute the pair potential energy in space between the two molecules.

Despite its non-unique nature, the local pressure tensor plays an important role in understanding the mechanical stability of lipid bilayers,^{20–23} proteins in glassy matrices,²⁴ and a liquid film suspended in the vapor.²⁵ For gas–liquid^{26,27} and liquid–solid^{28,29} nucleation, the local pressure profile provides a mechanical picture of the nano-nucleus and its interface and is useful for calculating the Tolman length for interfacial free energy.²⁸ In addition, the pressure tensor is required in the virial (or mechanical) route to the surface tension of planar,^{30,31} spherical,^{26,30} and cylindrical³² interfaces. Recently, the local pressure tensor has been used to characterize confined phases,^{33–35} motivated by high-pressure phenomena in adsorbed layers observed in both experiments and simulations.^{36,37} These high-pressure phenomena include chemical reactions that normally require a high pressure (e.g., 10 000 bars or more)^{38,39} and the formation/stabilization of a high-pressure phase structure^{40–43} in nanopores. The non-uniqueness of the local pressure, however, leads to confusion in interpreting the results and sometimes can lead to heated discussion.^{37,44}

In this paper, we consider the possibility of defining a coarse-grained pressure tensor that is independent of the integral contour chosen between molecules i and j by averaging the local pressure tensor, $\mathbf{P}(\mathbf{r})$, over some domain, $\Delta\mathbf{r}$, for a system of planar geometry (for example, a thin film adsorbed on a planar solid substrate or in a slit-shaped pore). We note that the coarse-grained pressure/stress tensors designed by Hardy,⁴⁵ Cormier *et al.*,⁴⁶ Ikeshoji *et al.*,⁴⁷ and Heinz⁴⁸ are essentially different from ours; the averaging volume in their definitions is unrestricted, and thus, the resulting coarse-grained pressure/stress can still be subject to the arbitrary choice of the integral contour. In Sec. II, we present the local pressure tensor equations for four arbitrary contour definitions for planar geometry, and we formulate a coarse-grained tangential pressure that is expected to be unique over some characteristic domain, $\Delta\mathbf{r}$. To support our argument, we performed grand canonical Monte Carlo (GCMC) simulations to investigate the local tangential pressure profile and its spatial integral of Lennard-Jones (LJ) argon adsorbed in a carbon slit-shaped pore. In Sec. III, simulation details are provided. In Sec. IV, we present a new method that allows for the calculation of the pressure integral (and the local pressure) using any arbitrary contour. Evidence from molecular simulations is presented to support the uniqueness of our coarse-grained tangential pressure. Based on the different length scales over which the coarse-grained tangential pressure appears to be unique, we can define the effective thickness of the layer and a statistical pore width. We report calculations of the coarse-grained in-layer and in-pore tangential pressure profiles for a range of pore widths and adsorbate–solid interaction strengths. In Sec. V, we summarize our findings.

II. THEORY

A. Local pressure tensor for planar geometry

For an interface of planar geometry lying in the xy -plane of Cartesian coordinates, it follows from symmetry considerations and the condition of mechanical stability [Eq. (1)] that the pressure

component normal to the surface, $P_N = P_{zz}$, is a constant and independent of z , as well as of x and y , and that the other two diagonal elements in the pressure tensor, $P_{xx}(z) = P_{yy}(z)$, represent the tangential pressure, $P_T(z)$, parallel to the surface. In the absence of strain, the off-diagonal elements are 0.

If the interactions are pairwise additive, the configurational contribution to the local pressure tensor by the virial route is given by^{5,49}

$$\mathbf{P}^C(\mathbf{r}) = \frac{1}{2} \left\langle \sum_{i \neq j} \mathbf{F}_{ij} \int_{C_{ij}} d\tilde{l} \delta(\mathbf{r} - \tilde{l}) \right\rangle, \quad (2)$$

where the angular bracket $\langle \dots \rangle$ indicates the ensemble average, \mathbf{F}_{ij} is the force vector between the ij particle pair, and the prefactor $1/2$ is to avoid double counting of particles. C_{ij} is an arbitrary contour connecting the ij -pair (in the direction from i to j), and $\delta(x)$ is the Dirac delta function. In Cartesian coordinates, Eq. (2) can be rewritten in the form

$$\mathbf{P}^C(\mathbf{r}) = \frac{1}{2} \left\langle \sum_{i \neq j} \frac{\mathbf{r}_{ij}}{r_{ij}} F_{ij} \int_{C_{ij}} d\tilde{l} \delta(x - x_l) \delta(y - y_l) \delta(z - z_l) \right\rangle, \quad (3)$$

where vector $\mathbf{r}_{ij} = \mathbf{r}_j - \mathbf{r}_i$, $F_{ij} = -du(r_{ij})/dr_{ij}$ is the ij -pair force, $u(r_{ij})$ is the pair potential between particles i and j separated by a scalar distance r_{ij} , and x_l , y_l , and z_l are Cartesian coordinates along the contour vector \tilde{l} .

The definition of the integral contour in Eq. (2) is not unique. Irving and Kirkwood (IK)² defined a straight line connecting the centers of the two molecules [see Fig. 1(a)]; if this line crosses the element of the surface, the pair force contributes to the pressure.

Due to its convenience for arbitrary geometry²⁴ and its consistency in different coordinate systems (spherical^{14,50} and cylindrical⁵¹), the IK definition of the contour has been widely accepted. The expression of the local tangential pressure by the IK definition can be written as^{31,52}

$$P_{T,IK}(z) = \rho(z)k_B T - \frac{1}{2S} \left\langle \sum_{i < j} \frac{x_{ij}^2 + y_{ij}^2}{r_{ij}} \frac{1}{|z_{ij}|} \frac{du(r_{ij})}{dr_{ij}} H\left(\frac{z - z_i}{|z_{ij}|}\right) H\left(\frac{z_j - z}{|z_{ij}|}\right) \right\rangle, \quad (4)$$

where S is the surface area of the xy -plane, $H(x)$ is the Heaviside step function, and x_{ij} , y_{ij} , and z_{ij} are the components of the vector \mathbf{r}_{ij} . The first term on the right-hand side of Eq. (4) is the kinetic contribution to the pressure, and the second term is the configurational contribution, averaged from P_{xx} and P_{yy} .

The other widely used definition of the integral contour is the Harasima (H) definition.^{6,7} It defines a path C_{ij} , first running from the position of particle i (x_i , y_i , z_i) in the direction parallel to the surface to the position (x_j , y_j , z_j) and then vertically to the position of particle j (x_j , y_j , z_j). The path, C_{ji} , starting from particle j is symmetric and equivalent to C_{ij} , as shown in Fig. 1(b). The H definition leads to a simpler local tangential pressure equation,³¹

$$P_{T,H}(z) = \rho(z)k_B T - \frac{1}{4S} \left\langle \sum_{i < j} \frac{x_{ij}^2 + y_{ij}^2}{r_{ij}} \frac{du(r_{ij})}{dr_{ij}} [\delta(z - z_i) + \delta(z - z_j)] \right\rangle. \quad (5)$$

The physical meaning of the delta function in Eq. (5) is that the configurational part only contributes to the tangential pressure at planes where molecules are present. This feature makes the H definition compatible with the non-pairwise reciprocal-space term in the Ewald summation method;^{22,51,53,54} thus, the H definition is preferred over the IK definition due to its computational efficiency in treating long-range electrostatic interactions. However, the H definition has also been shown to be inappropriate in polar coordinates due to the singularity at the polar origin.^{14,50,51} In practice, the delta function can be approximated as

$$\delta(z - z_i) = \lim_{\xi \rightarrow 0} \frac{1}{\xi} H[z - (z_i - \xi/2)] H[(z_i + \xi/2) - z]. \quad (6)$$

Apart from the IK and H definitions, we devised two additional integral contours for the local pressure tensor. One of them corresponds to a variation of the Irving–Kirkwood (IK-VR) definition. Figure 1(c) depicts the IK-VR definition of the integral contour. The contour C_{ij} goes from particle i vertically to point A of (x_i, y_i, z_A) , where $z_A = (z_i + 2z_j)/3$ is at a distance $2z_{ij}/3$ from particle i , and then straight to particle j . For the equivalent contour C_{ji} from particle j to particle i , as plotted in Fig. 1(c), we have $z_{A'} = (z_j + 2z_i)/3$. The final equation for the local tangential pressure is averaged from both contours C_{ij} and C_{ji} , and we have (see Appendix A for derivation)

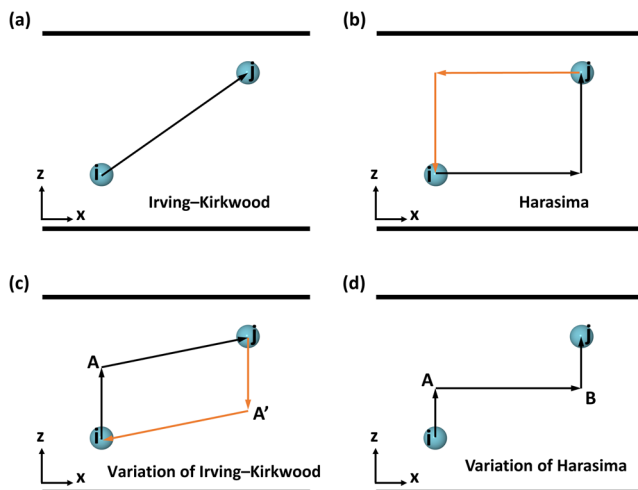


FIG. 1. Four different contour definitions for the local pressure tensor [Eq. (2)] in a planar geometry. (a) Irving–Kirkwood (IK) definition. (b) Harasima (H) definition. (c) A variation of the Irving–Kirkwood (IK-VR) definition. (d) A variation of the Harasima (H-VR) definition. For each definition, the contours C_{ij} (in black) and C_{ji} (in orange) are equivalent; since they overlap for the IK and H-VR definitions, only the contour C_{ij} is plotted for clarity. For each of these contours, the z_l values remain between z_i and z_j .

$$P_{T,IK-VR}(z) = \rho(z)k_B T - \frac{1}{4S} \left\langle \sum_{i < j} \frac{x_{ij}^2 + y_{ij}^2}{r_{ij}} \frac{du(r_{ij})}{dr_{ij}} \frac{3}{|z_{ij}|} \right. \\ \times \left. \left[H\left(\frac{z - z_A}{z_{ij}/3}\right) H\left(\frac{z_j - z}{z_{ij}/3}\right) + H\left(\frac{z_{A'} - z}{z_{ij}/3}\right) H\left(\frac{z - z_i}{z_{ij}/3}\right) \right] \right\rangle. \quad (7)$$

The other new contour that we devised in this work is a variation of the Harasima definition (H-VR), as shown in Fig. 1(d). The contour C_{ij} goes from particle i vertically to point A of (x_i, y_i, z_m) , where $z_m = (z_i + z_j)/2$ is the middle z -position between the ij -pair, then horizontally to point B (x_j, y_j, z_m) , and eventually to particle j . The local tangential pressure equation for this H-VR definition is (see Appendix A for derivation)

$$P_{T,H-VR}(z) = \rho(z)k_B T - \frac{1}{2S} \left\langle \sum_{i < j} \frac{x_{ij}^2 + y_{ij}^2}{r_{ij}} \frac{du(r_{ij})}{dr_{ij}} \delta\left(z - \frac{z_i + z_j}{2}\right) \right\rangle. \quad (8)$$

The equation to calculate the local normal pressure is the same for all the above contour definitions and is given by

$$P_N(z) = \rho(z)k_B T - \frac{1}{S} \left\langle \sum_{i < j} \frac{z_{ij}^2}{r_{ij}} \frac{1}{|z_{ij}|} \frac{du(r_{ij})}{dr_{ij}} H\left(\frac{z - z_i}{z_{ij}}\right) H\left(\frac{z_j - z}{z_{ij}}\right) \right\rangle. \quad (9)$$

Although the normal pressure in Eq. (9) is written as a function of the z -distance, it is essentially a unique constant throughout the system due to the mechanical equilibrium condition [Eq. (1)].

B. “Unique” coarse-grained pressure tensor for adsorbed layers

A common practice to avoid the non-uniqueness of the local pressure tensor is to average it over the entire system. From Eq. (2), it is straightforward to see that spatially averaging $\mathbf{P}^C(\mathbf{r})$ over the whole system space (to include all interacting pairs and contours) leads to a quantity that is independent of the arbitrary integral contour. For slit geometry, the pore wall is often modeled by an external field,

$$V_{ext}(D) = \varphi(D) + \varphi(H - D), \quad (10)$$

and the 10-4-3 Steele potential is taken for fluid-carbon wall interactions,⁵⁵

$$\varphi(D) = 2\pi\varepsilon_{as}\rho_s\sigma_{as}^2\Delta \left[\frac{2}{5} \left(\frac{\sigma_{as}}{D} \right)^{10} - \left(\frac{\sigma_{as}}{D} \right)^4 - \frac{\sigma_{as}^4}{3\Delta(D + 0.61\Delta)^3} \right], \quad (11)$$

where D is the distance of adsorbate sites from the graphite surface, ε_{as} and σ_{as} are the energy and size parameter for the adsorbate-solid interaction, ρ_s is the density of carbon atoms in graphite ($\rho_s = 0.114 \text{ \AA}^{-3}$), and Δ is the spacing between two adjacent graphene layers ($\Delta = 3.35 \text{ \AA}$). In this case, it is usual to average the local pressure tensor over the entire (physical) pore width H to give a unique in-pore pressure.⁵⁶ Here, we would like to take one step further to

explore the smallest domain over which the coarse-grained pressure tensor is unique, and meanwhile, we expect that this coarse-grained pressure tensor has direct physical significance, for example, representing the microscopic pressure for an adsorbed layer. Because the normal pressure component in the planar pressure tensor is well-defined, we focus on the tangential pressure component in the rest of this paper.

A typical density profile of an adsorbed fluid near a solid wall is shown in Fig. 2. In this subsection, for convenience, we assume that the wall is structureless and is modeled by an external field that only depends on the vertical distance to the flat surface [e.g., the 10-4-3 Steele potential in Eq. (11)]; thus, the wall potential does not contribute to the tangential pressure. We attempt to split the system into small bins, and each bin is designed to contain one density peak and has a width comparable to the thickness of the layer (see Fig. 2). A coarse-grained (cg) (in-layer) tangential pressure in the k th bin would be defined as

$$P_{T,k}^{cg} = \frac{1}{\Delta\mathbf{r}_k} \int_{\Delta\mathbf{r}_k} P_T(z) d\mathbf{r} \\ = \frac{1}{\Delta z_k} \int_{z_{0,k}}^{z_{0,k} + \Delta z_k} P_T(z) dz, \quad (12)$$

where $\Delta\mathbf{r}_k = S\Delta z_k$ is the volume of the k th bin and Δz_k is the characteristic length (or width) of the k th bin; $z_{0,k}$ is the lower bound of the k th bin. To make the coarse-grained tangential pressure defined in Eq. (12) unique, we have to find the integration range, $(z_{0,k}, z_{0,k} + \Delta z_k)$, over which the pressure integral in the numerator yields a unique value, regardless of the arbitrary contour definition adopted. This is equivalent to taking a spatial integration of the local tangential pressure, starting from the lower boundary of the system (in the z -direction), and locating, regardless of the contour definition chosen, points where the integral for the different contours converges; the integration range for Eq. (12) is then defined between proper convergence points. In what follows, we analyze the

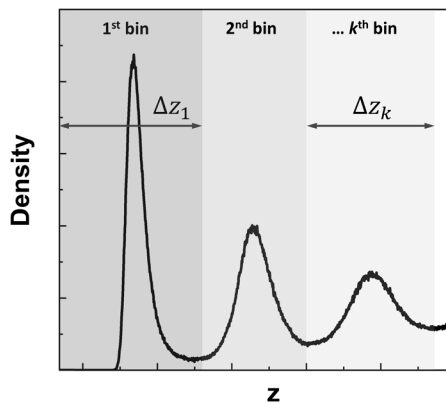


FIG. 2. A typical density profile of an adsorbed fluid near a solid planar wall. The system is binned in the z -direction normal to the solid wall for the calculation of the coarse-grained tangential pressure, and the bin width Δz_k for the k th bin ($k = 1, 2, \dots$) is comparable to the thickness of an adsorbed layer.

possibility of finding such convergence points in the pressure integral curve.

We can start from the configurational part of the xx -component tangential pressure in the pressure tensor [Eq. (A2) in Appendix A],

$$P_{xx}^C(z) = \frac{1}{2S} \left\langle \sum_{i \neq j} \frac{x_{ij}}{r_{ij}} F_{ij} \int_{C_{ij}} d\tilde{l}_x \delta(z - z_l) \right\rangle, \quad (13)$$

where \tilde{l}_x is the x -component of the contour vector. We now integrate Eq. (13) from the lower bound of the system, z_{wall} (the z -position of the solid wall), and we have

$$I(z) = \frac{1}{2S} \left\langle \sum_{i \neq j} \frac{x_{ij}}{r_{ij}} F_{ij} \int_{z_{wall}}^z dz' \int_{C_{ij}} d\tilde{l}_x \delta(z' - z_l) \right\rangle. \quad (14)$$

In this work, we assume that all valid contours for planar geometry are restricted to lie between the ij -pair (i.e., the contours follow values z_l between z_i and z_j); this avoids contours that pass through part of the adsorbent wall. We shall refer to such contours as “valid” contours in what follows. Before performing the integration with respect to the dummy variable z' in Eq. (14), we separate ij -pairs into three groups: (1) Group “A” contains the ij -pairs for which both molecule i and molecule j are within the integration range; thus, the contour connecting these two molecules satisfies $z_{wall} \leq z_l \leq z$. (2). Group “B” contains the ij -pairs for which one of the molecules in the pair (equivalently, a part of the contour) is outside the integration range. (3). Group “C” contains the ij -pairs for which both molecules in the pair are outside the integration range. For the first case, the integration with respect to z' is unity, i.e., $\int_{z_{wall}}^z dz' \delta(z' - z_l) = 1$. For the third case, the integration with respect to z' is 0 (since the delta function is 0). Equation (14) now can be rewritten as

$$I(z) = \frac{1}{2S} \left\langle \sum_{i \neq j}^A \frac{x_{ij}}{r_{ij}} F_{ij} \int_{C_{ij}} d\tilde{l}_x + \sum_{i \neq j}^B \frac{x_{ij}}{r_{ij}} F_{ij} \int_{z_{wall}}^z dz' \int_{C_{ij}} d\tilde{l}_x \delta(z' - z_l) \right\rangle. \quad (15)$$

The contour integral for the ij -pairs in Group “A” is simply $\int_{C_{ij}} d\tilde{l}_x = x_{ij}$. Carrying out the integration analytically for the ij -pairs in Group “B” leads to

$$\begin{aligned} I(z) &= \frac{1}{2S} \left\langle \sum_{i \neq j}^A \frac{x_{ij}^2}{r_{ij}} F_{ij} \right\rangle + \frac{1}{2S} \left\langle \sum_{i < j}^B \frac{x_{ij}}{r_{ij}} F_{ij} \left[\int_{z_{wall}}^z dz' \int_{C_{ij}} d\tilde{l}_x \delta(z' - z_l) \right. \right. \\ &\quad \left. \left. - \int_{z_{wall}}^z dz' \int_{C_{ji}} d\tilde{l}_x \delta(z' - z_l) \right] \right\rangle \\ &= \frac{1}{2S} \left\langle \sum_{i \neq j}^A \frac{x_{ij}^2}{r_{ij}} F_{ij} \right\rangle + \frac{1}{2S} \left\langle \sum_{i < j}^B \frac{x_{ij}^2}{r_{ij}} F_{ij} f_C[\lambda_{ij}(z)] \right\rangle, \end{aligned} \quad (16)$$

where

$$f_C[\lambda_{ij}(z)] = \begin{cases} (x_{in} + x_{im})/x_{ij} & z_i \leq z_j \\ (x_{jn} + x_{jm})/x_{ji} & z_i > z_j, \end{cases} \quad (17)$$

where point n and point m are intersections of contours C_{ij} and C_{ji} with the plane at position z , respectively, and x_{in} is the x -component of the vector \mathbf{r}_{in} , for example. Therefore, the value of the function defined in Eq. (17) depends on the arbitrarily valid contour (subscript “C” reminds us of this dependence). Given a contour definition, the function f_C is determined by $\lambda_{ij}(z) = (z - \min(z_i, z_j))/|z_{ij}|$, where $\min(\dots)$ returns the minimum value in a list of arguments, as is illustrated in Fig. 3(a). The interchange of the particle (molecule) identity in the ij -pair will not alter the value of $f_C[\lambda_{ij}(z)]$. By acknowledging that the contours C_{ij} and C_{ji} are equivalent and symmetric (due to the indistinguishability of particles i and j), we can show that the function f_C must satisfy the following conditions for any valid contour definition:

- (1) For ij -pairs in Group “B” [the second term on the right-hand side of Eq. (16)], the value of $\lambda_{ij}(z)$ ranges from 0 to 1, and the function must pass through points ($\lambda_{ij} = 0, f_C = 0$) and ($\lambda_{ij} = 1, f_C = 2$).
- (2) Function must pass through the middle point ($\lambda_{ij} = 0.5, f_C = 1$), as shown in Fig. 3(b).
- (3) Function must be symmetric about the middle point ($\lambda_{ij} = 0.5, f_C = 1$), i.e., $f_C(\lambda_{ij}) + f_C(1 - \lambda_{ij}) = 2$ (see Appendix B for proof).

We wish to evaluate the possibility of having convergence points in the integral curve, $I(z)$, such that, no matter what valid contour definition is used, the integral curve will always pass through those points. The first term on the right-hand side of Eq. (16) is unique, while the second term has the contour dependence included in the function f_C . Since f_C is coupled to the ij -pair forces, a rigorous proof of the existence of the convergence points that are independent of the contour definitions will be non-trivial, and the values for such convergence points are expected to be system-dependent. If we assume an extreme case where the density profile of each adsorbed layer behaves like a delta function (i.e., all molecules in the same layer lie on the same z -plane) and short-range interactions where only the nearest neighboring layers interact with each other, from the symmetric argument of the contour (see the second condition that f_C satisfies), it is obvious that the convergence point exists. In this case, the integration range that makes the coarse-grained tangential pressure [Eq. (12)] unique in the first adsorbed layer is $[z_{wall}, (z_1 + z_2)/2]$, where z_1 and z_2 are the z -positions of the first and the second layer, respectively, and here, the lower bound $z_{0,1}$ is chosen as

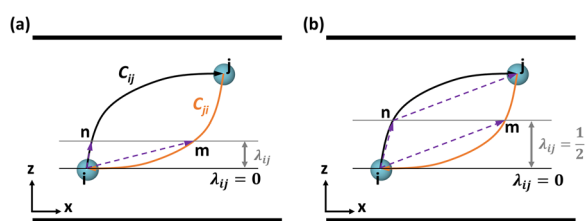


FIG. 3. Illustration for the calculation of function $f_C[\lambda_{ij}(z)]$ defined in Eq. (17), in the case of $z_i \leq z_j$, for (a) the general situation and (b) the situation where $\lambda_{ij} = 0.5$ and $f_C = 1$, where $\lambda_{ij}(z) = (z - \min(z_i, z_j))/|z_{ij}|$. Point n and point m are intersections of arbitrarily valid contours C_{ij} and C_{ji} with the z -plane, respectively.

z_{wall} . For real cases, it would be interesting to integrate the local tangential pressure numerically to see if the convergence points exist. This will help justify the uniqueness of the coarse-grained tangential pressure.

In the rest of this paper, we will first evaluate Eq. (16) numerically using more than ten types of valid contour definitions for LJ argon confined in a structureless slit pore, modeled by Eqs. (10) and (11). For a more realistic system where the solid wall is modeled by a fully atomistic one, the contribution to the local tangential pressure from the adsorbate–solid interactions will be accounted for. We calculate the local tangential pressure explicitly using IK, H, IK-VR, and H-VR definitions in realistic pore models and investigate the corresponding pressure integral.

III. SIMULATION DETAILS

Grand canonical Monte Carlo (GCMC) simulations⁵⁷ were carried out to model LJ argon adsorbed in carbon slit-shaped pores at $T = 87.3$ K and $P_{bulk} = 1$ bar. The chemical potentials of the adsorbate (μ), pore volume (V), and temperature (T) were fixed in the simulation. The adsorbate–adsorbate (aa) interaction was represented by the 12-6 LJ potential,

$$u(r) = 4\epsilon_{aa} \left[\left(\frac{\sigma_{aa}}{r} \right)^{12} - \left(\frac{\sigma_{aa}}{r} \right)^6 \right], \quad (18)$$

where $\epsilon_{aa}/k_B = 119.8$ K is the LJ energy parameter and $\sigma_{aa} = 3.405$ Å is the LJ diameter for argon molecules. For the structureless pore model, Eqs. (10) and (11) were used in the simulation. For a more realistic pore model, the pore wall was represented as rigid graphite with three perfect graphene sheets stacked in an ABA pattern parallel to the xy -plane. Graphene sheets were spaced 3.35 Å apart. Two graphite solid blocks were placed in symmetry about the pore center at $z = 0$ to simulate a semi-infinite slit-shaped pore. The lateral dimensions of the pore surface were set to 68×34.08 Å². An open space having a size (in the x -direction) of 60 Å was added to both ends of the pore so that the pore has direct contact with the bulk phase. Periodic boundary conditions were applied in both x - and y -directions, and the hard-wall boundary condition was used for the z -direction. A schematic plot of the realistic pore model is drawn in Fig. 4(a). The interactions between the LJ argon and the pore atoms were modeled in the same way as that of adsorbate–adsorbate interactions but with aa interaction parameters replaced by the adsorbate–solid (as) interaction parameters. The LJ parameters for carbon atoms⁵⁵ were taken to be $\sigma_{ss} = 3.4$ Å and $\epsilon_{ss}/k_B = 28.0$ K, and the cross-diameter σ_{as} was calculated from the Lorentz combining rule,⁵⁸ i.e., $\sigma_{as} = (\sigma_{aa} + \sigma_{ss})/2$. The cross-energy parameter, ϵ_{as} , was adjusted to give a particular value of the wetting parameter,^{59,60} which is a measurement of the degree to which the adsorbate wets the wall,

$$\alpha_w = \rho_s \sigma_{as}^2 \Delta \left(\frac{\epsilon_{as}}{\epsilon_{aa}} \right). \quad (19)$$

We investigated cases where the wetting parameter α_w equals 1, 2.14 (corresponding to Ar/graphite based on the Berthelot combining rule,⁶¹ $\epsilon_{as} = \sqrt{\epsilon_{aa}\epsilon_{ss}}$), and 5, mimicking the physisorption

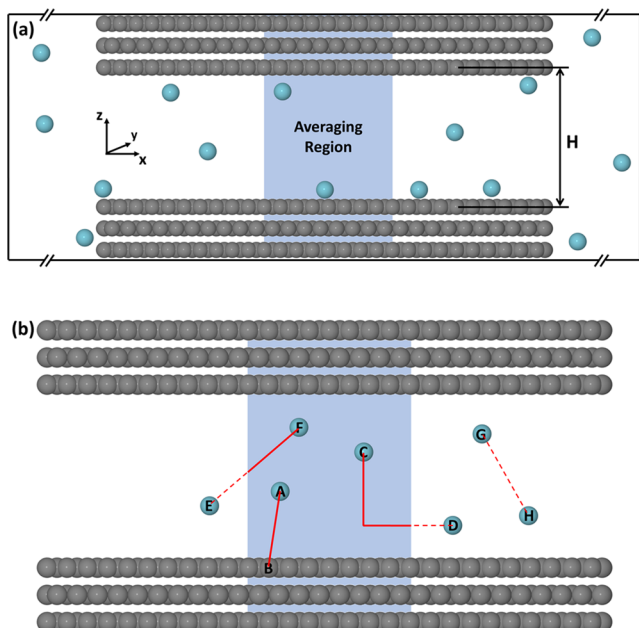


FIG. 4. (a) Schematic plot of the simulation box for a realistic pore model. Physical pore width is H . The blue region is the averaging region (with a length of $\sim 5\sigma_{aa}$ in the x -direction) where the sampling was performed. The averaging region was placed deep inside of the pore; thus, the pore edge effects were negligible. Cyan particles are LJ argon, and gray particles are solid atoms. (b) Illustrative examples of calculating the local pressure tensor in the averaging region. If both particles in the pair are inside the averaging region, such as the A–B interaction, its contribution to the local pressure tensor can be calculated by the standard equations. If either one of the interacting particles is outside the averaging region, only the contour that is inside the region should be accounted for, such as the solid line part for the C–D interaction (H definition) and for the E–F interaction (IK definition). If both particles in the pair are outside the averaging region, such as the G–H interaction, it does not contribute to the pressure tensor.

behavior from a weakly wetting one to a strongly wetting one. The cutoff radius for the 12-6 LJ potential was chosen as $r_c = 5\sigma_{aa}$, which was large enough to neglect the impulsive contribution to the pressure.^{16,51}

The statistics (e.g., the local pressure tensor and the pressure integral) were sampled in the entire simulation box and in the averaging region (see Fig. 4) for the structureless pore model and the realistic pore model, respectively. To calculate the local pressure tensor in the realistic pore model, the averaging region was divided into small bins in the z -direction with bin width $w = 0.01$ Å, and the parameter ξ in Eq. (6) was set equal to the bin width w . Examples of calculating the local pressure tensor in the averaging region are illustrated in Fig. 4(b). Displacement, insertion, and deletion moves were first attempted with equal probability to fill the pore; the probability of attempting a displacement move was then improved to 0.98 to further equilibrate the condensed system for at least 5×10^7 moves. Statistics were collected from the following 2×10^7 – 5×10^7 configurations. Multiple independent runs for each system were performed to enhance statistics. The chemical potential of argon in the bulk phase was calculated by the Lennard-Jones

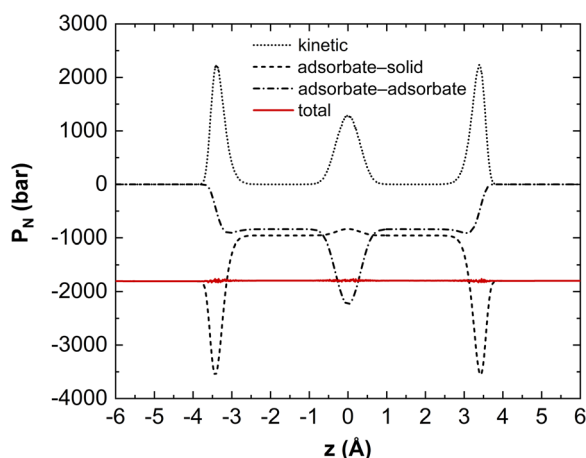


FIG. 5. Local normal pressure profile for argon adsorption in a realistic carbon slit pore with $H = 4\sigma_{aa}$ and $\alpha_w \approx 2.14$, at 87.3 K and a bulk pressure of 1 bar. The total normal pressure is decomposed into the kinetic and configurational (adsorbate–solid and adsorbate–adsorbate) contributions. Since the pore wall was treated as a rigid one, the solid–solid contribution to the pressure profile is neglected. The total normal pressure is a constant within statistical uncertainties throughout the pore, confirming the mechanical equilibrium of the system.

equation of state.⁶² We monitored the local normal pressure for each slit pore system using Eq. (9) and observed that the normal pressure is a constant within statistical uncertainties, confirming that all systems have reached mechanical equilibrium inside the pore (see Fig. 5, for example).

IV. RESULTS AND DISCUSSIONS

A. Numerical evidence for the uniqueness of the coarse-grained tangential pressure

In this section, we provide numerical evidence from molecular simulation to show that it is possible to find an appropriate integration domain over which the coarse-grained tangential pressure defined in Eq. (12) has a unique value.

1. Structureless carbon slit pore

To calculate Eq. (16) from molecular simulation, we need to construct the function $f_C(\lambda_{ij})$ first. The exact form of $f_C(\lambda_{ij})$ depends on the choice of contour definition. According to the IK, H, IK-VR, and H-VR definitions, we can write out the corresponding form for $f_C(\lambda_{ij})$, that is, one contour definition maps to one functional form (i.e., one-to-one mapping from three-dimensional space to a two-dimensional xz -plane; see Fig. 3). In addition, we devised another six types of valid contours and write out the corresponding forms for $f_C(\lambda_{ij})$. Graphs of different functional forms are shown in Fig. 6, and the mathematical formulas are presented in Table I. It should be noted that there is a one-to-many mapping from a functional form of $f_C(\lambda_{ij})$ to the corresponding contours in three-dimensional space. Therefore, by calculating Eq. (16) using ten types of $f_C(\lambda_{ij})$,

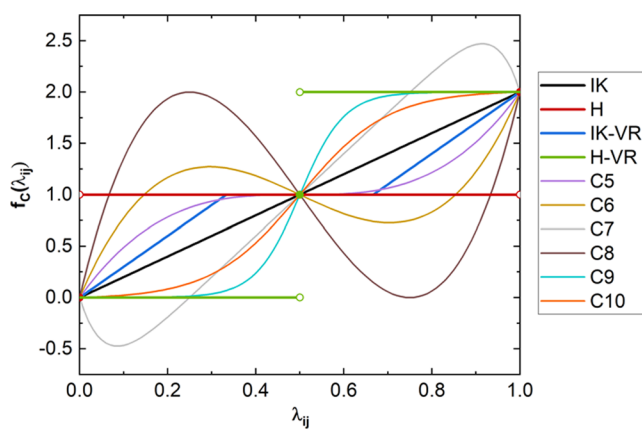


FIG. 6. Graphs of function $f_C(\lambda_{ij})$ that correspond to different contour definitions. Mathematical formulas for the function are listed in Table I.

we are essentially investigating the properties of more than ten types of contour definitions.

Figure 7 shows the density profile and the pressure integral [Eq. (16)] using different contour definitions for LJ argon confined in a structureless carbon slit pore of $H = 10\sigma_{aa}$ and $\alpha_w \approx 2.14$. As predicted by Eq. (2), integrating the local tangential pressure over the entire system to include all pairwise interactions leads to a

TABLE I. Mathematical formulas for function $f_C(\lambda_{ij})$ that corresponds to different types of contour definitions. Graphs of this function are shown in Fig. 6.

Contour definitions	$f_C(\lambda_{ij})$
IK	$2\lambda_{ij}$
H	$\begin{cases} 0 & \lambda_{ij} = 0 \\ 1 & \lambda_{ij} \in (0, 1) \\ 2 & \lambda_{ij} = 1 \end{cases}$
IK-VR	$\begin{cases} 3\lambda_{ij} & \lambda_{ij} \in [0, 1/3] \\ 1 & \lambda_{ij} \in [1/3, 2/3] \\ 3\lambda_{ij} - 1 & \lambda_{ij} \in (2/3, 1] \end{cases}$
H-VR	$\begin{cases} 0 & \lambda_{ij} \in [0, 0.5] \\ 1 & \lambda_{ij} = 0.5 \\ 2 & \lambda_{ij} \in (0.5, 1] \end{cases}$
C5	$8(\lambda_{ij} - 0.5)^3 + 1$
C6	$16(\lambda_{ij} - 0.5)^3 - 2\lambda_{ij} + 2$
C7	$-2^9(\lambda_{ij} - 0.5)^9 + 4\lambda_{ij} - 1$
C8	$2^5(\lambda_{ij} - 0.5)^3 - 6(\lambda_{ij} - 0.5) + 1$
C9	$\frac{1}{\tanh(5)} \tanh\left(\frac{\lambda_{ij} - 0.5}{0.1}\right) + 1$
C10	$\frac{1}{\tanh(2.5)} \tanh\left(\frac{\lambda_{ij} - 0.5}{0.2}\right) + 1$

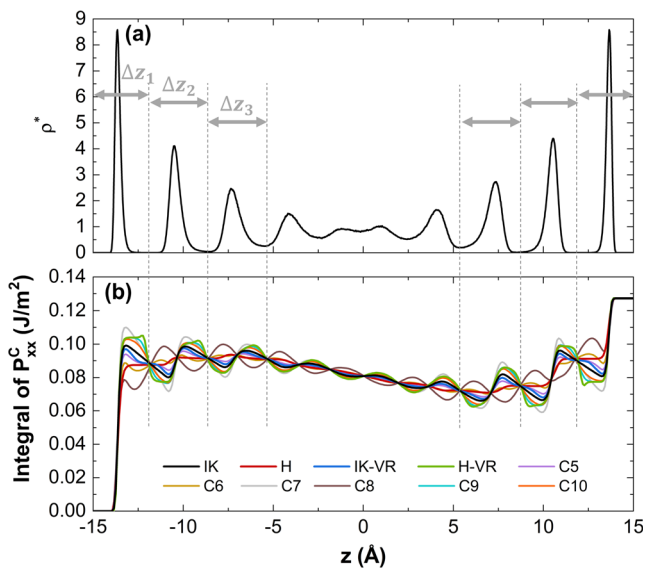


FIG. 7. (a) Reduced local number density profile $\rho^* = \rho\sigma_{aa}^3$ and (b) the spatial integral of configurational contribution to the local tangential pressure [Eq. (16)] using different contour definitions for LJ argon adsorption in a structureless carbon slit pore with $H = 10\sigma_{aa}$ and $\alpha_w \approx 2.14$, at 87.3 K and a bulk pressure of 1 bar. The characteristic length (integration range) that can lead to a unique coarse-grained in-layer tangential pressure is marked in the plot.

convergent value that is independent of the arbitrarily valid contour definitions. Interestingly, we observe that all integral curves pass through the same point at a certain distance (within numerical uncertainty), indicating that it is possible to formulate a unique coarse-grained tangential pressure defined between those convergence points (see characteristic lengths, Δz_k , $k = 1, 2, \dots$, marked in Fig. 7). We observed similar converging behavior of the pressure integral curves at other wetting parameters and narrower pores. Moreover, the gradient of the pressure integral curve determines the local tangential pressure. The sharp increase in the integral curve near the structureless surface in Fig. 7(b) corresponds to a positive peak of the local tangential pressure (here, only the configurational contribution is accounted for), indicating strong repulsion between molecules in the first adsorbed layer near the wall. Calculating the local tangential pressure by differentiating Eq. (16) is advantageous: without defining the contour explicitly, it allows us to explore the entire valid contour space by creating appropriate functional forms for $f_C(\lambda_{ij})$, as long as the new form satisfies the three conditions listed in Sec. II B. This method can easily be extended to other components in the pressure tensor.

2. Realistic carbon slit pore

For realistic carbon slit pores, instead of adapting Eq. (16) to the new system, we calculated the local tangential pressure using the conventional method (i.e., using the pressure equations in Sec. II A), and the corresponding spatial integrals are then obtained from these local values. Figure 8(a) shows a full-range local tangential

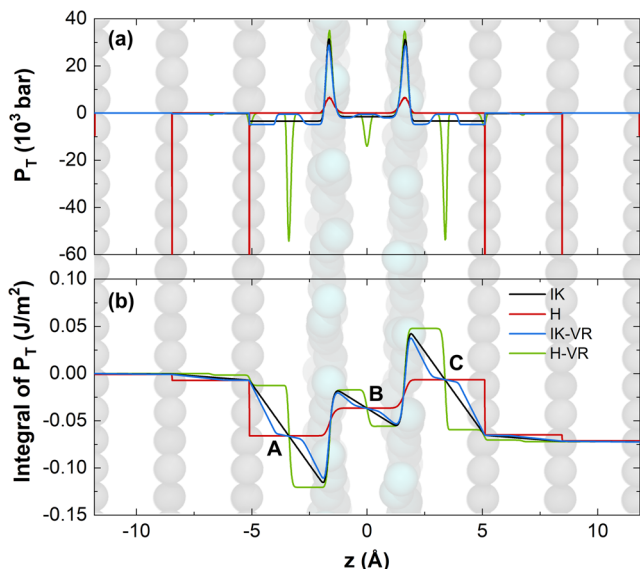


FIG. 8. (a) Local tangential pressure profile by different contour definitions (IK, H, IK-VR, and H-VR) and (b) the corresponding spatial integral for argon adsorption in a realistic carbon slit pore with $H = 3\sigma_{aa}$ and $\alpha_w \approx 2.14$, at 87.3 K and a bulk pressure of 1 bar. A simulation snapshot is shown in the background, and the particles are drawn at reduced scale for clarity; cyan particles in the center are argon molecules, and gray particles are solid atoms. Peaks of the local tangential pressure for IK, IK-VR, and H-VR definitions are similar and overlap. Points "A" to "C" in (b) are intersections of the four integral curves, and the integration range for the coarse-grained tangential pressure in an adsorbed layer should be (z_A, z_B) , for example.

pressure profile (including the region of the pore wall) by four different contour definitions for LJ argon adsorbed in an atomistic carbon slit pore of $H = 3\sigma_{aa}$ and $\alpha_w \approx 2.14$. The local tangential pressure includes both kinetic and configurational contributions. As expected, different contour definitions lead to distinct local tangential pressures. The positive pressure peak values for IK, IK-VR, and H-VR definitions are similar in magnitude, while the H definition shows a relatively lower peak value. The formation of the dense layer is due to the strong attractive force field exerted by the carbon wall.³⁷ A negative tangential pressure is present in the region between the adsorbed layer and the wall ($2.5 \text{ \AA} \lesssim |z| \lesssim 5 \text{ \AA}$). Because the H definition only assigns the local pressure to the position where a molecule/atom is located, negative pressure pulses are observed at the z -position of the graphene sheets. A negative pressure is also observed between two adsorbed layers by the IK, IK-VR, and H-VR definitions, indicating that two layers are in tension.

The integration of the local tangential pressure from the lower bound of the system, $\int_{-L_{hf}}^z P_T(z') dz'$, where $L_{hf} = (H + 4\Delta)/2$ and Δ is the spacing between two graphene sheets, is shown in Fig. 8(b). We observe that these integral curves do not resemble the ones for the structureless model because, in addition to the adsorbate–adsorbate interaction, the adsorbate–solid interaction also now comes into play. Nonetheless, the shape of the integral curve for each contour

definition inside the pore is still qualitatively unchanged regardless of pore models. As expected, the pressure integral curves by four different contour definitions also converge at some points. The z -position of convergence points “A,” “B,” and “C” marked in Fig. 8(b) represents the desired lower/upper integration bounds for the coarse-grained in-layer tangential pressure defined in Eq. (12). The convergent behavior of the integral curves at a certain distance in Fig. 8(b) is general. In Fig. 9, we present two examples for larger pores ($H = 4\sigma_{aa}$ and $H = 7\sigma_{aa}$). The local tangential pressure and

its corresponding numerical integral profiles in Fig. 9 are plotted in a magnified view for clarity, from the first convergent point to the last one inside the pore [e.g., from z_A to z_C in Fig. 8(b)]. By referring to the density profile, we can clearly identify the convergent points in the integral profile that correspond to the lower/upper bounds in the calculation of the unique coarse-grained tangential pressure. We noticed that the integral curves of the local tangential pressure by different contour definitions do not converge exactly to the same points in calculations due to errors in the numerical integration (Trapezoidal rule) and uncertainties in the molecular simulation. However, the extent by which the four integral curves deviate from the “averaged” convergent point is of the same order of magnitude as the numerical error when integrating the local tangential pressure over the entire system, while in the latter case, we know that all integral curves will converge to the same value. Due to the sharp increase in the integral curves, it is also hard for us to identify the convergence points that appear near some density peaks (see the contact layer near the wall in Fig. 8, for example). Nevertheless, the results provide convincing evidence that it is possible to define a coarse-grained tangential pressure over a well-defined domain, and this pressure appears to be unique and independent of the valid contour definition in the local pressure tensor.

B. Effective thickness of the adsorbed layer and the statistical pore width

The thickness of the first adsorbed layer near the solid wall is an important parameter in controlling the kinetics,⁶³ thermodynamics,⁶⁴ and structure^{65,66} of adsorption systems. It can also be used to define the boundary between the adsorbed phase and the bulk gas phase in theoretical models.^{67,68} However, the determination of this quantity is still impeded by the lack of an objective and unique definition of the concept of the “molecular thickness.” The possibility to uniquely define a coarse-grained pressure tensor we have shown in Sec. IV A provides a new perspective to solve this ambiguity. The characteristic length for the k th layer, Δz_k , can be thought of as the effective thickness of the layer. From the numerical integration results from Sec. IV A, we can readily determine this characteristic length. In particular, the characteristic length for the first adsorbed layer near the realistic pore wall, Δz_1 , at different pore widths and wetting parameters is shown in Fig. 10. For small pores ($H \lesssim 3\sigma_{aa}$), the value of Δz_1 is almost identical for all wetting parameters studied. With the increase in the pore width, the effective thickness of the first adsorbed layer is slightly larger for $\alpha_w = 1$ than for 2.14 and is slightly smaller for $\alpha_w = 5$, which has the fastest decaying rate among the three. This is because for large pores, the adsorbed layer has more freedom to adjust its structure according to the adsorbate–solid interaction strength, without being restricted by the pore geometry. The stronger the adsorbate–solid interaction is, the more ordered and compact the layer structure will be. The effective thickness of the first layer in Fig. 10 ($0.8\sigma_{aa} \sim 1.1\sigma_{aa}$) is in good agreement with the reported values based on the density profile,⁶⁹ mean-field criteria,⁶⁷ and IR measurement.⁷⁰ Our approach to determine the effective thickness of the monolayer has the following advantages over the current methods: (1) it is applicable to any pore width (from the micropore to open surface), (2) there are no empirical criteria (e.g., threshold, “dead space”) involved, and (3) it is unified within the framework of statistical

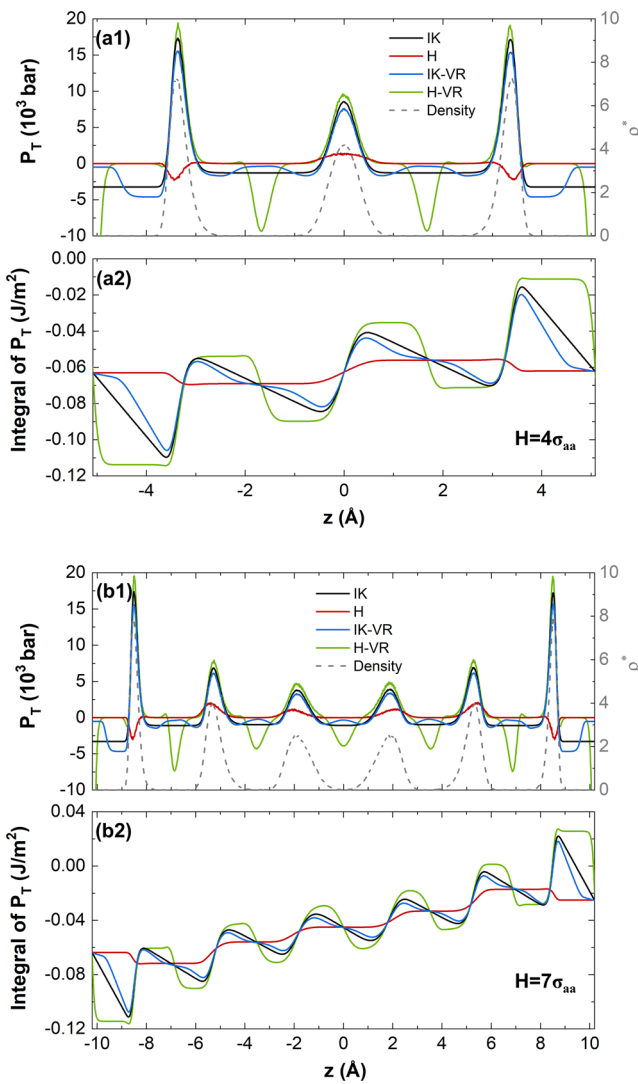


FIG. 9. Local tangential pressure profile by different contour definitions (IK, H, IK-VR, and H-VR, upper panel) and the corresponding integral (bottom panel) for argon adsorption in a realistic carbon slit pore with (a) $H = 4\sigma_{aa}$, (b) $H = 7\sigma_{aa}$, and wetting parameter $\alpha_w \approx 2.14$, at 87.3 K and a bulk pressure of 1 bar. The density profiles of argon (dashed line) in reduced units are also plotted (read on the right-hand vertical scale in a1 and b1), where $\rho^* = \rho\sigma_{aa}^{-3}$. The profiles are plotted in a range from the first convergent point to the last one inside the pore.

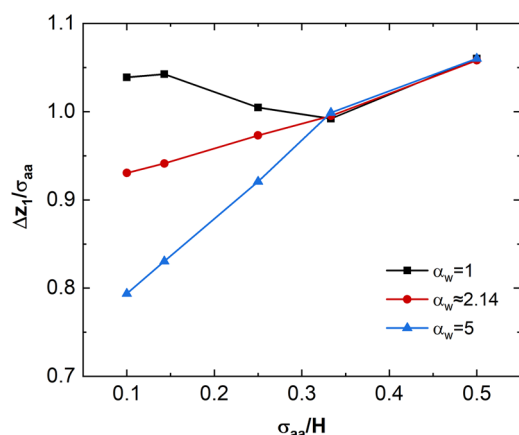


FIG. 10. The characteristic length (or effective thickness) for the first adsorbed layer near the pore wall, Δz_1 , vs σ_{aa}/H at different wetting parameters for argon adsorption in a realistic carbon slit pore at 87.3 K and a bulk pressure of 1 bar. The lines are drawn to guide the eye.

mechanics. However, the applicability of the approach depends on whether the unique coarse-grained pressure concept is valid in the system of interest.

In addition to the in-layer tangential pressure that is spatially averaged over a single layer, we can also define an in-pore tangential pressure by spatially averaging the local tangential pressure over the two convergent points that delimit the boundary of the nano-pore within which all adsorbed layers are included [e.g., from z_A to z_C in Fig. 8(b)]. Accordingly, a statistical pore width and a pore volume that is conjugate to the in-pore tangential pressure can be determined. We collected the statistical pore widths for different wetting parameters and compare them with other pore size definitions in Fig. 11. Here, we consider three common choices for the pore size definition: (1) The physical pore width, H , is the definition that we adopt in this work to characterize our pore model [see Fig. 4(a)]. (2) The effective pore width allows for the “dead space” near the wall, which is inaccessible to the centers of the adsorbate molecules. This “dead space,” z_{min} , can be estimated by setting the mean-field potential in Eq. (11) to 0,⁶⁹ i.e., $\varphi(z_{min}) = 0$. We find $z_{min} \approx 2.89 \text{ \AA}$ for LJ argon adsorbed on a graphite surface with Lorentz–Berthelot combining rules applied, and the effective pore width is $H_{eff} = H - 2z_{min}$. (3) The internal pore width simply refers to the space between “hard-sphere” wall carbon atoms, and it is given by $H_{in} = H - \sigma_{ss}$. It is clear from Fig. 11 that the statistical width is in good agreement with the internal width and deviates from the physical and effective widths. Our results support and rationalize the use of the internal pore width in modern molecular methods for characterizing the pore size distribution.^{71–73} It should be noted that the internal pore width is not equivalent to the statistical width but just a good approximation to it. The internal width is purely geometric, while the statistical width is related to the intermolecular interactions. It has been argued that a modified internal pore width based on the adsorbate–solid potential appears to be more satisfactory than the geometric one in reproducing experimental adsorption isotherms.⁷⁴

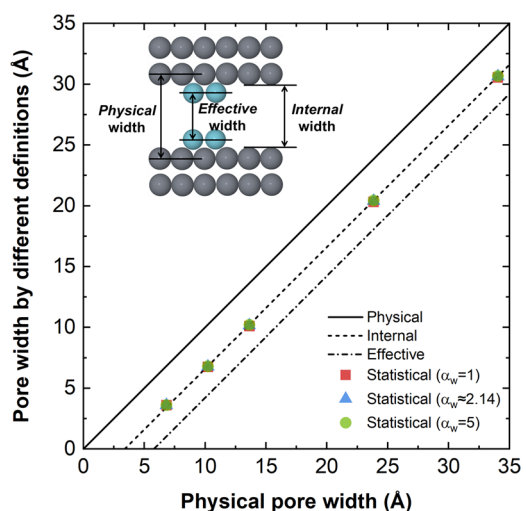


FIG. 11. Comparison of the statistical pore width that is consistent with the coarse-grained in-pore tangential pressure with three common definitions for the pore width. The statistical pore width is calculated for LJ argon in a realistic carbon slit pore with three different wetting parameters, α_w , at 87.3 K and a bulk pressure of 1 bar. See the main text for details.

It is apparent that the thermodynamic and transport properties of confined fluids are sensitive to the pore width (especially for small pores). This definition of the statistical width is expected to reduce ambiguities and improve the consistency of the calculated properties in nano-confinement.

C. Coarse-grained tangential pressure profile in realistic carbon slit pores

Equipped with all appropriate length scales and integration ranges, we can calculate the “unique” coarse-grained in-layer and in-pore tangential pressure for different physical pore widths. These are shown in Fig. 12 in comparison with the local tangential pressure by two commonly used contour definitions. The local tangential pressure profiles for all wetting parameters at a certain pore width are qualitatively similar; thus, in what follows, we focus on the case of $\alpha_w \approx 2.14$. The pressure profiles for $\alpha_w = 1$ and $\alpha_w = 5$ are shown in Appendix C for the reader’s reference.

Figure 12 shows that, again, different contour definitions for the local pressure tensor lead to an ambiguous picture of the mechanical state of the adsorbed phase inside the pore. Specifically, for pores of H/σ_{aa} equal to 4 and 7, the IK profile shows a positive local pressure for the first adsorbed layer, while the H definition predicts a negative local value. This seemingly contradictory picture has also been observed in more complex systems, such as the polymeric thin films confined between two repulsive walls⁷⁵ and water inside a carbon nanotube.⁵¹ With the help of the coarse-grained tangential pressure, a “unique” pressure value for the first adsorbed layer can be revealed, and it is negative (~ -200 bars) for $H = 4\sigma_{aa}$ and $H = 7\sigma_{aa}$. For the other pore widths examined, the in-layer tangential pressure for the first adsorbed layer is positive. The sign of the in-layer tangential

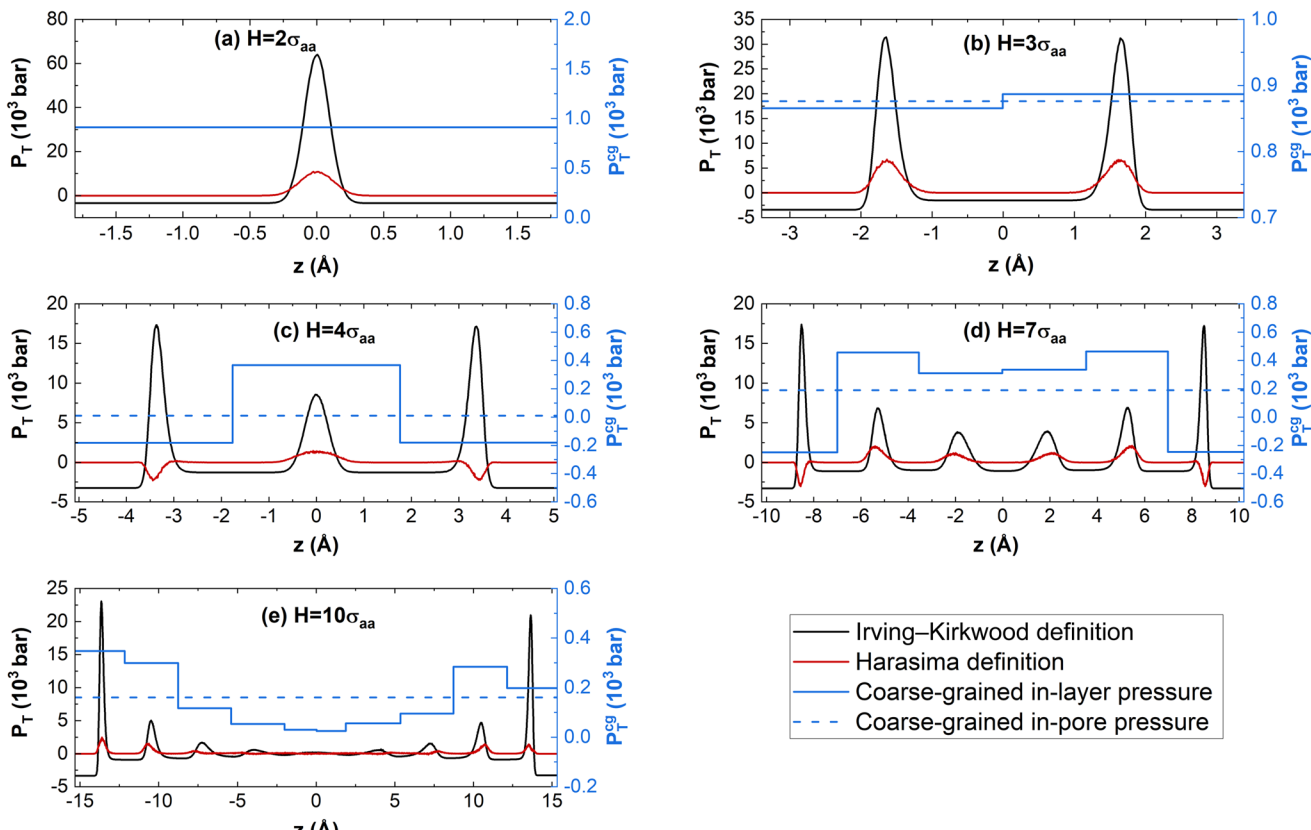


FIG. 12. Local tangential pressure profile (P_T , read on the left-hand vertical scale) by the IK and H definitions in comparison with the coarse-grained tangential pressure (P_T^{cg} , read on the right-hand vertical scale) that appears to be unique for argon adsorption in realistic carbon slit pores of reduced physical pore widths H/σ_{aa} of 2, 3, 4, 7, and 10, at 87.3 K and a bulk pressure of 1 bar. The systems are for a wetting parameter of $\alpha_w \approx 2.14$. Note that for $H = 2\sigma_{aa}$, with only one adsorbed layer, the coarse-grained in-layer and in-pore pressures are identical. The asymmetric in-layer profile is due to the fact that the simulated in-pore structure is not perfectly symmetric.

pressure can be explained by the competition between the compression of the molecules inside the layer and the main attractive force from the pore wall. If the adsorbed layer is not dense enough and the repulsion between the molecules in the layer cannot compensate for the attractive forces exerted by the pore wall and by the neighboring layers, the tangential pressure inside the first layer is negative (see also Fig. 14, for example). When we increase the adsorbate–solid interactions (or, for small pores, when the potentials from the two walls overlap), a more compact first adsorbed layer will form. Since the repulsive force increases exponentially as two adsorbate molecules approach each other,³⁷ at some point, the compression inside the first layer outweighs the attraction from the wall and neighboring layers and the in-layer tangential pressure becomes positive (see Fig. 15, for example). Because the middle layers are less impacted by the attractive pore walls, the in-layer tangential pressure is always positive in the middle layers but with a decaying trend toward the pore center, where a bulk-like phase tends to form in large pores. Except for the case of $H = 4\sigma_{aa}$, the overall in-pore pressure in Fig. 12 shows an augmentation of about two to three orders of magnitude over the bulk pressure (1 bar). This

provides solid evidence for pressure enhancement inside the pore when the fluid strongly wets the surface, although the currently reported enhancement is weaker than that based on the non-unique local pressure.³³ It is clear that this pressure enhancement is more prominent for stronger adsorbate–solid interactions (see Fig. 15). It is worth noting that the coarse-grained in-layer tangential pressure here is different from the layer-by-layer representation of the stress tensor by Sega *et al.*⁷⁶ The latter relies on the H definition to distribute the virials to each particle in the layers.

V. CONCLUSIONS

In their paper in 1950, Irving and Kirkwood² remarked: “When averaging (the local stress tensor) over a domain large compared with the range of intermolecular force, these differences are washed out, and the ambiguity remaining in the microscopic stress tensor is of negligible order.” In this work, we have presented a new method that defines a coarse-grained pressure by integration of the local pressure tensor using any valid contour definitions; the corresponding

local pressure can be obtained by differentiating the integral curve. This new method allows us, in principle, to explore the entire valid contour space. The molecular simulation results have been presented for a LJ fluid confined in both structureless and realistic carbon slit pores of various widths and wetting parameter values, which allows for the determination of the integration of the local tangential pressure using the new method and the conventional method. We have shown that for LJ fluids near a solid wall, it is possible to define such a “unique,” coarse-grained (or spatially averaged) tangential pressure by averaging the local tangential pressure over some well-defined range. Two length scales that correspond to the coarse-grained tangential pressure for an adsorbed layer (in-layer pressure) and for the entire pore (in-pore pressure) can be regarded as the effective thickness of the adsorbed layer and the statistical pore width, respectively. In particular, the effective thickness of the first adsorbed layer near the wall is about one LJ diameter, depending on the pore width and wetting parameter, and compares favorably with other reported values. The statistical pore width is smaller than the physical pore width but is well estimated by the internal pore width, which is a common pore width definition used in the adsorption field. The calculated coarse-grained tangential pressure profile inside the pore provides an unambiguous mechanical picture of the adsorbed phase and results in a better understanding of the pressure enhancement for strongly wetting systems.

While the coarse-grained tangential pressure introduced here should be applicable to a wide range of planar interface applications, we note several likely restrictions. The chosen contour should be physically sensible, i.e., it should not pass through the solid adsorbent. We have, therefore, proposed that the contour should be confined to the z -space lying between the two molecules i and j and we refer to such contours as “valid” contours, as Irving and Kirkwood cautioned.² Second, the adsorbate should sufficiently wet the solid so that layering occurs. This is the case for the results presented here (α_w values of 1 and above). However, for very weakly wetting systems, such as mercury on carbon ($\alpha_w \sim 0.1$), we do not expect layering. Third, the results presented here are for planar surfaces and intermolecular forces of short range. Future studies will focus on the possibility of defining a “unique” coarse-grained pressure tensor for curved surfaces and longer-ranged forces, particularly for Coulomb forces.

Finally, we note that the ability to define a microscopic, coarse-grained pressure and the corresponding length scale unequivocally may help to establish a thermodynamically consistent description of highly inhomogeneous systems, and to bridge the gap between experiment and theory in comparing microscopic properties. However, a more rigorous (mathematical) proof is desired in the future to identify the true convergence points in the pressure integral curve for any valid contour definitions, and further evidence is needed to support the existence of this “unique” coarse-grained pressure tensor.

ACKNOWLEDGMENTS

We thank Dr. Yun Long and Professor Gerald (Jerry) Wang for helpful discussions. This work was supported, in part, by the U.S. National Science Foundation under Grant No. CBET-1603851.

APPENDIX A: DERIVATION FOR THE LOCAL TANGENTIAL PRESSURE BY THE IK-VR AND H-VR DEFINITIONS

We start with the component P_{xx} in the pressure tensor. Because the local tangential pressure only depends on the z -position perpendicular to the planar interface, we perform an average over the x - and y -direction first to integrate out unnecessary variables. For the configurational (C) part of the local tangential pressure P_{xx} , we have

$$P_{xx}^C(z) = \frac{1}{S} \int_0^{L_x} dx \int_0^{L_y} dy [\hat{e}_x \cdot \mathbf{P}^C \cdot \hat{e}_x], \quad (A1)$$

where $S = L_x L_y$ and \mathbf{P}^C is the second-order pressure tensor given in Eq. (3); \hat{e}_x is the unit vector in the x -direction. The integral limits, L_x and L_y , represent the simulation box size in the x - and y -direction, respectively, if the pressure tensor is sampled over the entire simulation box. They can also represent the size in the x - and y -direction for a specified averaging region (see Fig. 4) if the pressure tensor is only sampled over that space. Substituting Eq. (3) into Eq. (A1) gives

$$\begin{aligned} P_{xx}^C(z) &= \frac{1}{2S} \left\langle \sum_{i \neq j} \int_0^{L_x} dx \int_0^{L_y} dy \frac{\hat{e}_x \cdot \mathbf{r}_{ij}}{r_{ij}} F_{ij} \right. \\ &\quad \times \int_{C_{ij}} d\tilde{l} \cdot \hat{e}_x \times \delta(x - x_l) \delta(y - y_l) \delta(z - z_l) \Big\rangle \\ &= \frac{1}{2S} \left\langle \sum_{i \neq j} \frac{x_{ij}}{r_{ij}} F_{ij} \int_{C_{ij}} d\tilde{l} \cdot \hat{e}_x \times \delta(z - z_l) \right\rangle. \end{aligned} \quad (A2)$$

In the following derivations, we assume that the entire contour C_{ij} (or C_{ji}) is inside the space where the pressure tensor will be sampled (and this is the normal case if the sampling is performed over the entire simulation box). We will also discuss the situation where only part of the contour is inside the averaging region [see examples in Fig. 4(b)] at the end of this Appendix.

For the IK-VR definition [see Fig. 1(c)], the contour vector \tilde{l} starting from particle i can be expressed as

$$\tilde{l} = \mathbf{r}_i + \alpha \mathbf{r}_{iA} + \beta \mathbf{r}_{Aj}, \quad (A3)$$

where $\{\alpha, \beta\}$ ranges from $[0, 1]$. The differentiation of the contour \tilde{l} gives

$$d\tilde{l} = \mathbf{r}_{iA} d\alpha + \mathbf{r}_{Aj} d\beta. \quad (A4)$$

Substituting Eq. (A4) into Eq. (A2) leads to

$$P_{xx}^C(z) = \frac{1}{2S} \left\langle \sum_{i \neq j} \frac{x_{ij}^2}{r_{ij}} F_{ij} \int_0^1 \delta(z - z_l) d\beta \right\rangle, \quad (A5)$$

where $z_l = z_A + \beta z_{Aj}$. Applying the identities,

$$\int_0^1 f(\beta) d\beta = \int_{-\infty}^{+\infty} f(\beta) H(\beta) H(1 - \beta) d\beta, \\ \delta[f(\beta)] = \sum_k \frac{1}{|f'(\beta_k)|} \delta(\beta - \beta_k), \quad (A6)$$

where $f'(\beta) = df/d\beta$ and β_k is a simple root of $f(\beta_k) = 0$, Eq. (A5) yields

$$P_{xx}^C(z) = \frac{1}{2S} \left\langle \sum_{i \neq j} \frac{x_{ij}^2}{r_{ij}} F_{ij} \int_{-\infty}^{+\infty} H(\beta) H(1 - \beta) \delta(z - z_l) d\beta \right\rangle \\ = \frac{1}{2S} \left\langle \sum_{i \neq j} \frac{x_{ij}^2}{r_{ij}} F_{ij} \int_{-\infty}^{+\infty} H(\beta) H(1 - \beta) \frac{1}{|z_{Aj}|} \delta(\beta - \beta_k) d\beta \right\rangle \\ = \frac{1}{2S} \left\langle \sum_{i \neq j} \frac{x_{ij}^2}{r_{ij}} F_{ij} \frac{3}{|z_{ij}|} H\left(\frac{z - z_A}{z_{ij}/3}\right) H\left(\frac{z_j - z}{z_{ij}/3}\right) \right\rangle. \quad (A7)$$

Similarly, for the configurational tangential pressure in the y -direction, we have

$$P_{yy}^C(z) = \frac{1}{2S} \left\langle \sum_{i \neq j} \frac{y_{ij}^2}{r_{ij}} F_{ij} \frac{3}{|z_{ij}|} H\left(\frac{z - z_A}{z_{ij}/3}\right) H\left(\frac{z_j - z}{z_{ij}/3}\right) \right\rangle. \quad (A8)$$

Due to the symmetry of the system in the xy -plane ($P_{xx} = P_{yy}$), the final expression for the local tangential pressure is averaged from P_{xx} and P_{yy} to enhance statistics. By adding up the kinetic contribution and writing the summation in a more efficient way (i.e., $i < j$), we have

$$P_{T,IK-VR}(z) = \rho(z) k_B T - \frac{1}{4S} \left\langle \sum_{i < j} \frac{x_{ij}^2 + y_{ij}^2}{r_{ij}} \frac{du(r_{ij})}{dr_{ij}} \frac{3}{|z_{ij}|} \times \left[H\left(\frac{z - z_A}{z_{ij}/3}\right) H\left(\frac{z_j - z}{z_{ij}/3}\right) + H\left(\frac{z_{A'} - z}{z_{ij}/3}\right) H\left(\frac{z - z_i}{z_{ij}/3}\right) \right] \right\rangle, \quad (A9)$$

where the scalar force, F_{ij} , is replaced by $-du(r_{ij})/dr_{ij}$ and $z_A = (z_i + 2z_j)/3$, $z_{A'} = (z_j + 2z_i)/3$.

For the H-VR definition [see Fig. 1(d)], we can write the contour vector \tilde{l} starting from particle i as

$$\tilde{l} = \mathbf{r}_i + \alpha \mathbf{r}_{iA} + \beta \mathbf{r}_{AB} + \gamma \mathbf{r}_{Bj} \\ = \mathbf{r}_i + \alpha(\mathbf{r}_A - \mathbf{r}_i) + \beta(\mathbf{r}_B - \mathbf{r}_A) + \gamma(\mathbf{r}_j - \mathbf{r}_B), \quad (A10)$$

where $\{\alpha, \beta, \gamma\}$ ranges from $[0, 1]$. The differentiation of the contour \tilde{l} gives

$$d\tilde{l} = \mathbf{r}_{iA} d\alpha + \mathbf{r}_{AB} d\beta + \mathbf{r}_{Bj} d\gamma. \quad (A11)$$

Substituting the differential of the integral contour [Eq. (A11)] into Eq. (A2) and noting that $\mathbf{r}_{iA} \cdot \hat{\mathbf{e}}_x = \mathbf{r}_{Bj} \cdot \hat{\mathbf{e}}_x = 0$ lead to

$$P_{xx}^C(z) = \frac{1}{2S} \left\langle \sum_{i \neq j} \frac{x_{ij}}{r_{ij}} F_{ij} \int_0^1 \mathbf{r}_{AB} \cdot \hat{\mathbf{e}}_x \times \delta(z - z_m) d\beta \right\rangle \\ = \frac{1}{2S} \left\langle \sum_{i \neq j} \frac{x_{ij}}{r_{ij}} F_{ij} \delta\left(z - \frac{z_i + z_j}{2}\right) \right\rangle. \quad (A12)$$

Similarly,

$$P_{yy}^C(z) = \frac{1}{2S} \left\langle \sum_{i \neq j} \frac{y_{ij}}{r_{ij}} F_{ij} \delta\left(z - \frac{z_i + z_j}{2}\right) \right\rangle. \quad (A13)$$

The final expression for the local tangential pressure by the H-VR definition is

$$P_{T,H-VR}(z) = \rho(z) k_B T - \frac{1}{2S} \left\langle \sum_{i < j} \frac{x_{ij}^2 + y_{ij}^2}{r_{ij}} \frac{du(r_{ij})}{dr_{ij}} \delta\left(z - \frac{z_i + z_j}{2}\right) \right\rangle. \quad (A14)$$

In the case where part of the integral contour is inside the averaging region, then only that inside part of the contour should be accounted for in the pressure calculation. Mathematically, for example, the integration with respect to β in Eq. (A5) now should not be carried out from 0 to 1 (entire range) but rather over a range representing the part of the contour vector \tilde{l} that is inside the averaging region.

APPENDIX B: MATHEMATICAL PROOF OF FUNCTION $f_C[\lambda_{ij}(z)]$ BEING SYMMETRIC ABOUT THE POINT ($\lambda_{ij} = 0.5$, $f_C = 1$)

Considering the situation in Fig. 13, we have

$$2 - f_C(1 - \lambda_{ij}) = 2 - \frac{x_{iN} + x_{iM}}{x_{ij}} = \frac{2x_{ij} - (x_{iN} + x_{iM})}{x_{ij}}. \quad (B1)$$

The symmetry of the arbitrary contour C_{ij} and C_{ji} leads to

$$x_{in} + x_{iM} = x_{im} + x_{iN} = x_{ij}. \quad (B2)$$

Combining Eqs. (B1) and (B2), we have

$$2 - f_C(1 - \lambda_{ij}) = \frac{2x_{ij} - (x_{iN} + x_{iM})}{x_{ij}} = \frac{x_{im} + x_{in}}{x_{ij}} = f_C(\lambda_{ij}). \quad (B3)$$

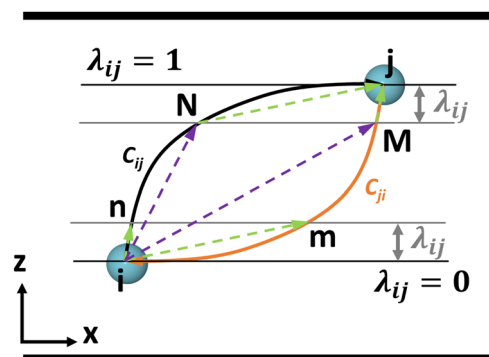


FIG. 13. Illustration for the calculation of function $f_C(\lambda_{ij})$ defined in Eq. (17) in the case of $z_i \leq z_j$. Points n and m are intersections of arbitrarily valid contours with the plane corresponding to λ_{ij} , and points N and M are intersections of contours with the plane corresponding to $(1 - \lambda_{ij})$.

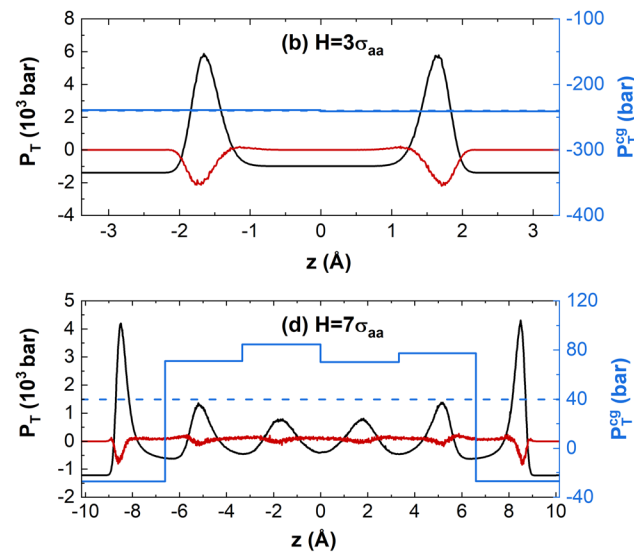
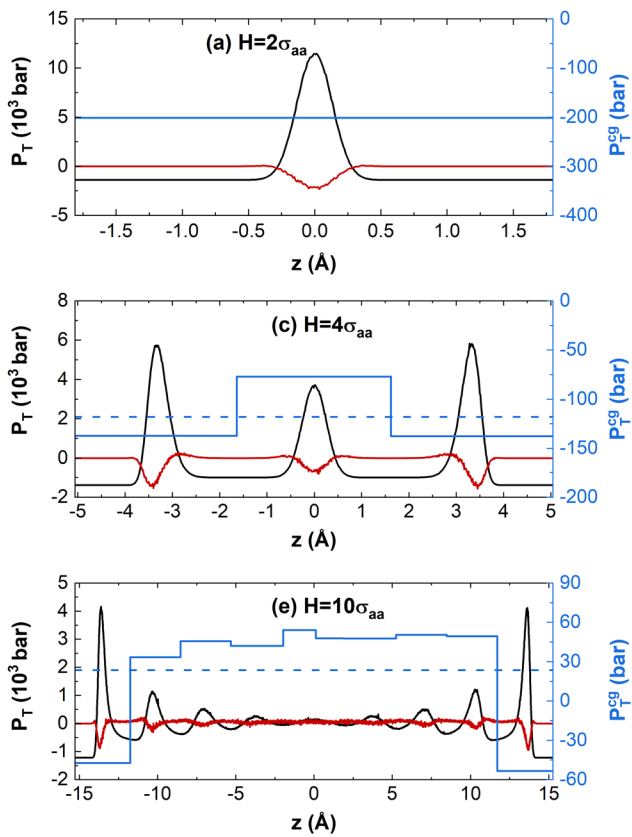
Therefore, we have proved that the function $f_C(\lambda_{ij})$ is symmetric about the point $(\lambda_{ij} = 0.5, f_C = 1)$.

APPENDIX C: COARSE-GRAINED TANGENTIAL PRESSURE PROFILE FOR $\alpha_w = 1$ AND $\alpha_w = 5$

The local tangential pressure profile by the IK and H definitions in comparison with the coarse-grained tangential pressure that appears to be unique are presented in Fig. 14 and Fig. 15 for wetting parameters of 1 and 5, respectively, for argon adsorption in realistic carbon slit pores of reduced physical pore widths H/σ_{aa} of 2, 3, 4, 7, and 10, at 87.3 K and a bulk pressure of 1 bar.

DATA AVAILABILITY

The data that support the findings of this study are available from the corresponding author upon reasonable request.



- Irving–Kirkwood definition
- Harasima definition
- Coarse-grained in-layer pressure
- - - Coarse-grained in-pore pressure

FIG. 14. Local tangential pressure profile (P_T , read on the left-hand vertical scale) by the IK and H definitions in comparison with the coarse-grained tangential pressure (P_T^{cg} , read on the right-hand vertical scale) that appears to be unique for argon adsorption in realistic carbon slit pores of reduced physical pore widths H/σ_{aa} of 2, 3, 4, 7 and 10, at 87.3 K and a bulk pressure of 1 bar. The systems are for a wetting parameter of $\alpha_w = 1$. The asymmetric in-layer profile is due to the fact that the simulated in-pore structure is not perfectly symmetric.

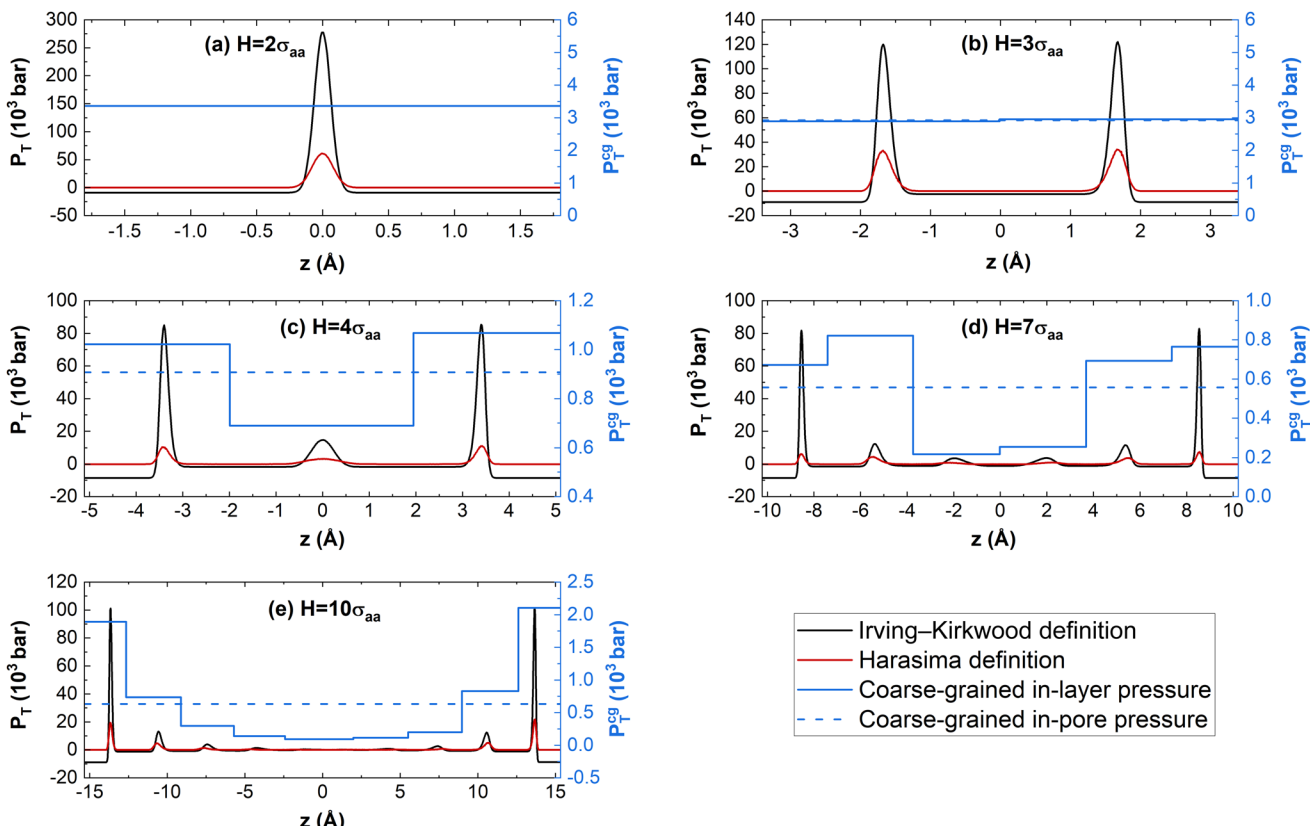


FIG. 15. Local tangential pressure profile (P_T , read on the left-hand vertical scale) by the IK and H definitions in comparison with the coarse-grained tangential pressure (P_T^{cg} , read on the right-hand vertical scale) that appears to be unique for argon adsorption in realistic carbon slit pores of reduced physical pore widths H/σ_{aa} of 2, 3, 4, 7 and 10, at 87.3 K and a bulk pressure of 1 bar. The systems are for a wetting parameter of $\alpha_w = 5$. The asymmetric in-layer profile is due to the fact that the simulated in-pore structure is not perfectly symmetric.

REFERENCES

- ¹R. B. Griffiths and J. C. Wheeler, *Phys. Rev. A* **2**, 1047 (1970).
- ²J. H. Irving and J. G. Kirkwood, *J. Chem. Phys.* **18**, 817 (1950).
- ³J. C. Maxwell, *Nature* **17**, 278 (1878).
- ⁴L. Boltzmann, in *The Kinetic Theory of Gases: An Anthology of Classic Papers with Historical Commentary*, History Of Modern Physical Sciences Vol. 1 (Imperial College Press, 2003), pp. 392–402.
- ⁵P. Schofield and J. R. Henderson, *Proc. R. Soc. A* **379**, 231 (1982).
- ⁶J. G. Kirkwood and F. P. Buff, *J. Chem. Phys.* **17**, 338 (1949).
- ⁷A. Harasima, *Advances in Chemical Physics* (Wiley & Sons, Inc., 1958), pp. 203–237.
- ⁸L. Mistura, *Int. J. Thermophys.* **8**, 397 (1987).
- ⁹M. Baus and R. Lovett, *Phys. Rev. Lett.* **65**, 1781 (1990).
- ¹⁰J. S. Rowlinson, *Phys. Rev. Lett.* **67**, 406 (1991).
- ¹¹M. Baus and R. Lovett, *Phys. Rev. Lett.* **67**, 407 (1991).
- ¹²M. Baus and R. Lovett, *Phys. Rev. A* **44**, 1211 (1991).
- ¹³E. Wajnryb, A. R. Altenberger, and J. S. Dahler, *J. Chem. Phys.* **103**, 9782 (1995).
- ¹⁴B. Hafskjold and T. Ikeshoji, *Phys. Rev. E* **66**, 011203 (2002).
- ¹⁵G. C. Rossi and M. Testa, *J. Chem. Phys.* **132**, 074902 (2010).
- ¹⁶E. de Miguel and G. Jackson, *J. Chem. Phys.* **125**, 164109 (2006).
- ¹⁷Y. Long, *Pressure Tensor of Adsorbate in Nanoporous Materials: Molecular Simulation Studies* (North Carolina State University, 2012).
- ¹⁸Y. Long, J. C. Palmer, B. Coasne, M. Śliwińska-Bartkowiak, G. Jackson, E. A. Müller, and K. E. Gubbins, *J. Chem. Phys.* **139**, 144701 (2013).
- ¹⁹A. Ghoufi and P. Malfreyt, *Mol. Simul.* **39**, 603 (2013).
- ²⁰R. Goetz and R. Lipowsky, *J. Chem. Phys.* **108**, 7397 (1998).
- ²¹R. H. Templer, S. J. Castle, A. Rachael Curran, G. Rumbles, and D. R. Klug, *Faraday Discuss.* **111**, 41 (1999).
- ²²J. Sonne, F. Y. Hansen, and G. H. Peters, *J. Chem. Phys.* **122**, 124903 (2005).
- ²³J. M. Vanegas, A. Torres-Sánchez, and M. Arroyo, *J. Chem. Theory Comput.* **10**, 691 (2014).
- ²⁴H. W. Hatch and P. G. Debenedetti, *J. Chem. Phys.* **137**, 035103 (2012).
- ²⁵J.-G. Weng, S. Park, J. R. Lukes, and C.-L. Tien, *J. Chem. Phys.* **113**, 5917 (2000).
- ²⁶S. M. Thompson, K. E. Gubbins, J. P. R. B. Walton, R. A. R. Chantry, and J. S. Rowlinson, *J. Chem. Phys.* **81**, 530 (1984).
- ²⁷P. R. ten Wolde and D. Frenkel, *J. Chem. Phys.* **109**, 9901 (1998).
- ²⁸K. G. S. H. Gunawardana and X. Song, *J. Chem. Phys.* **148**, 204506 (2018).
- ²⁹P. Montero de Hijes, K. Shi, E. G. Noya, E. E. Santiso, K. E. Gubbins, E. Sanz, and C. Vega, *J. Chem. Phys.* **153**, 191102 (2020).
- ³⁰J. S. Rowlinson and B. Widom, *Molecular Theory of Capillarity* (Clarendon Press, Oxford, 1982).
- ³¹J. P. R. B. Walton, D. J. Tildesley, J. S. Rowlinson, and J. R. Henderson, *Mol. Phys.* **48**, 1357 (1983).
- ³²C. K. Addington, Y. Long, and K. E. Gubbins, *J. Chem. Phys.* **149**, 084109 (2018).

- ³³Y. Long, J. C. Palmer, B. Coasne, M. Śliwińska-Bartkowiak, and K. E. Gubbins, *Phys. Chem. Chem. Phys.* **13**, 17163 (2011).
- ³⁴C. K. Addington, J. M. Mansell, and K. E. Gubbins, *Mol. Simul.* **43**, 519 (2017).
- ³⁵D. Srivastava, C. H. Turner, E. E. Santiso, and K. E. Gubbins, *J. Phys. Chem. B* **122**, 3604 (2018).
- ³⁶K. E. Gubbins, K. Gu, L. Huang, Y. Long, J. M. Mansell, E. E. Santiso, K. Shi, M. Śliwińska-Bartkowiak, and D. Srivastava, *Engineering* **4**, 311 (2018).
- ³⁷Y. Long, J. C. Palmer, B. Coasne, K. Shi, M. Śliwińska-Bartkowiak, and K. E. Gubbins, *Phys. Chem. Chem. Phys.* **22**, 9826 (2020).
- ³⁸K. Kaneko, N. Fukuzaki, K. Kakei, T. Suzuki, and S. Ozeki, *Langmuir* **5**, 960 (1989).
- ³⁹K. S. Vasu, E. Prestat, J. Abraham, J. Dix, R. J. Kashtiban, J. Beheshtian, J. Sloan, P. Carbone, M. Neek-Amal, S. J. Haigh, A. K. Geim, and R. R. Nair, *Nat. Commun.* **7**, 12168 (2016).
- ⁴⁰J. Regnier, A. Thomy, and X. Duval, *J. Colloid Interface Sci.* **70**, 105 (1979).
- ⁴¹H. Abou-Rachid, A. Hu, V. Timoshevskii, Y. Song, and L.-S. Lussier, *Phys. Rev. Lett.* **100**, 196401 (2008).
- ⁴²K. Urita, Y. Shiga, T. Fujimori, T. Iiyama, Y. Hattori, H. Kanoh, T. Ohba, H. Tanaka, M. Yudasaka, S. Iijima, I. Moriguchi, F. Okino, M. Endo, and K. Kaneko, *J. Am. Chem. Soc.* **133**, 10344 (2011).
- ⁴³T. Fujimori, A. Morelos-Gómez, Z. Zhu, H. Muramatsu, R. Futamura, K. Urita, M. Terrones, T. Hayashi, M. Endo, S. Young Hong, Y. Chul Choi, D. Tománek, and K. Kaneko, *Nat. Commun.* **4**, 2162 (2013).
- ⁴⁴D. van Dijk, *Phys. Chem. Chem. Phys.* **22**, 9824 (2020).
- ⁴⁵R. J. Hardy, *J. Chem. Phys.* **76**, 622 (1982).
- ⁴⁶J. Cormier, J. M. Rickman, and T. J. Delph, *J. Appl. Phys.* **89**, 99 (2001).
- ⁴⁷T. Ikeshoji, B. Hafskjold, and H. Furuholt, *Mol. Simul.* **29**, 101 (2003).
- ⁴⁸H. Heinz, *Mol. Simul.* **33**, 747 (2007).
- ⁴⁹C. G. Gray, K. E. Gubbins, and C. G. Joslin, in *Theory of Molecular Fluids*, Applications Vol. 2 (Oxford University Press, 2011), pp. 928–942.
- ⁵⁰E. M. Blokhuis and D. Bedeaux, *J. Chem. Phys.* **97**, 3576 (1992).
- ⁵¹K. Shi, Y. Shen, E. E. Santiso, and K. E. Gubbins, *J. Chem. Theory Comput.* **16**, 5548 (2020).
- ⁵²M. Rao and B. J. Berne, *Mol. Phys.* **37**, 455 (1979).
- ⁵³J. Alejandre, D. J. Tildesley, and G. A. Chapela, *J. Chem. Phys.* **102**, 4574 (1995).
- ⁵⁴M. Segá, B. Fábián, and P. Jedlovszky, *J. Chem. Theory Comput.* **12**, 4509 (2016).
- ⁵⁵W. A. Steele, *Surf. Sci.* **36**, 317 (1973).
- ⁵⁶Y. Hamada, K. Koga, and H. Tanaka, *Physica A* **388**, 2289 (2009).
- ⁵⁷D. Frenkel and B. Smit, *Understanding Molecular Simulation: From Algorithms to Applications*, 2nd ed. (Academic Press, San Diego, 2002).
- ⁵⁸H. A. Lorentz, *Ann. Phys.* **248**, 127 (1881).
- ⁵⁹R. Radhakrishnan, K. E. Gubbins, and M. Śliwińska-Bartkowiak, *J. Chem. Phys.* **112**, 11048 (2000).
- ⁶⁰K. E. Gubbins, Y. Long, and M. Śliwińska-Bartkowiak, *J. Chem. Thermodyn.* **74**, 169 (2014).
- ⁶¹D. Berthelot, *Compt. Rendus* **126**, 1703 (1898).
- ⁶²J. K. Johnson, J. a. Zollweg, and K. E. Gubbins, *Mol. Phys.* **78**, 591 (1993).
- ⁶³G. J. Wang and N. G. Hadjiconstantinou, *Langmuir* **34**, 6976 (2018).
- ⁶⁴S. Sun, H. Xu, J. Han, Y. Zhu, B. Zuo, X. Wang, and W. Zhang, *Soft Matter* **12**, 8348 (2016).
- ⁶⁵C. Tiemeyer, A. Lange, and J. Plank, *Colloids Surf., A* **456**, 139 (2014).
- ⁶⁶Y. F. Houst, P. Bowen, F. Perche, A. Kauppi, P. Borget, L. Galmiche, J.-F. Le Meins, F. Lafuma, R. J. Flatt, I. Schober, P. F. G. Banfill, D. S. Swift, B. O. Myrvold, B. G. Petersen, and K. Reknes, *Cem. Concr. Res.* **38**, 1197 (2008).
- ⁶⁷A. Martinez, M. Castro, C. McCabe, and A. Gil-Villegas, *J. Chem. Phys.* **126**, 074707 (2007).
- ⁶⁸Y. Tian, C. Yan, and Z. Jin, *Sci. Rep.* **7**, 12040 (2017).
- ⁶⁹G. J. Wang and N. G. Hadjiconstantinou, *Phys. Rev. Fluids* **2**, 094201 (2017).
- ⁷⁰D. B. Asay and S. H. Kim, *J. Phys. Chem. B* **109**, 16760 (2005).
- ⁷¹P. N. Aukett, N. Quirke, S. Riddiford, and S. R. Tennison, *Carbon* **30**, 913 (1992).
- ⁷²N. Setoyama, T. Suzuki, and K. Kaneko, *Carbon* **36**, 1459 (1998).
- ⁷³P. I. Ravikovich, A. Vishnyakov, R. Russo, and A. V. Neimark, *Langmuir* **16**, 2311 (2000).
- ⁷⁴K. Kaneko, R. F. Cracknell, and D. Nicholson, *Langmuir* **10**, 4606 (1994).
- ⁷⁵F. Varnik, J. Baschnagel, and K. Binder, *J. Chem. Phys.* **113**, 4444 (2000).
- ⁷⁶M. Segá, B. Fábián, and P. Jedlovszky, *J. Chem. Phys.* **143**, 114709 (2015).